

# Gain engineering and topological atom laser in synthetic dimensions

Takuto Tsuno,<sup>1</sup> Shintaro Taie,<sup>1,\*</sup> Yosuke Takasu,<sup>1</sup> Kazuya Yamashita,<sup>1</sup> Tomoki Ozawa,<sup>2</sup> and Yoshiro Takahashi<sup>1</sup>

<sup>1</sup>*Department of Physics, Graduate School of Science, Kyoto University, Kyoto 606-8502, Japan*

<sup>2</sup>*Advanced Institute for Materials Research (WPI-AIMR), Tohoku University, Sendai 980-8577, Japan*

(Dated: April 23, 2024)

## ABSTRACT

In the recent rapid progress of quantum technology, controlling quantum states has become an important subject of study. Of particular interest is the control of open quantum systems, where the system of interest couples to the environment in an essential way. One formalism to describe open systems is the non-Hermitian quantum mechanics. Photonics systems have been a major platform to study non-Hermitian quantum mechanics due to its flexibility in engineering gain and loss. Ultracold atomic gases have also used to study non-Hermitian quantum mechanics. However, unlike in photonics, gain is not easily controllable in ultracold atomic gases, and exploration of non-Hermitian physics has been limited to control of losses. In this paper, we report engineering of effective gain through evaporative cooling of judiciously chosen initial thermal atoms. We observe resulting formation of Bose-Einstein condensation (BEC) in excited eigenstates of a synthetic lattice. We realize formation of BEC in a topological edge state of the Su-Schrieffer-Heeger lattice in the synthetic hyperfine lattice, which can be regarded as atomic laser oscillations at a topological edge mode, i.e. topological atom laser. Gain-loss engineering in ultracold atoms opens a novel prospect to explore open many-body quantum systems.

## INTRODUCTION

With the recent rapid progress in the development of quantum technology, there is an increasing interest in controlling open quantum systems<sup>1</sup>. One important framework in describing open quantum systems is the non-Hermitian quantum mechanics<sup>2,3</sup>. Dating back to the study of nuclear decay<sup>4</sup>, non-Hermitian quantum mechanics has been rediscovered and studied in various contexts. One turning point is the discovery of parity-time reversal ( $\mathcal{PT}$ )-symmetric Hamiltonians<sup>5,6</sup>, which, despite being non-Hermitian, give rise to real energy spectrum. Another very recent development came from understanding of the topological properties of non-Hermitian Hamiltonians<sup>7,8</sup>. Since non-Hermitian Hamiltonians generally have complex eigenenergies, modes with positive imaginary part can lead to amplification and lasing. Topological laser, which is a laser whose lasing mode is a topological edge mode, has been realized<sup>9–15</sup>, and its potential application in integrated photonics has been actively

pursued<sup>16</sup>. In quantum many-body systems coupled to the environment, an effective description in terms of non-Hermitian Hamiltonians is possible in the quantum trajectory approach between quantum jumps<sup>17,18</sup>, and the effect of non-Hermiticity in many-body quantum phases have been actively studied<sup>19–33</sup>.

Since its experimental realization of  $\mathcal{PT}$ -symmetric optics in 2009<sup>34–36</sup>, non-Hermitian quantum mechanics has been actively studied in optics<sup>37–39</sup>. Despite the huge success, optical systems have a limitation that the interaction is typically classical nonlinearity, making it difficult to study quantum many-body physics in non-Hermitian setups. An emerging platform to study non-Hermitian quantum mechanics is ultracold atomic gases, where one can study quantum many-body physics in a controlled manner<sup>40–42</sup>. Recently, there has been experiments in which non-Hermitian Hamiltonian has been realized by controlling dissipation in ultracold atomic gases<sup>43,44</sup>. However, ultracold atomic gases have its own limitation that the non-Hermiticity that can be introduced has been limited to the control of dissipation. It has thus been not possible to study non-Hermitian physics related to controlled gain in ultracold atomic gases. Without gain, it is not possible to study phenomena related to amplification and lasing.

Here we report engineering of gain in ultracold atomic gases and observe the formation of Bose-Einstein condensation (BEC) in an excited eigenstate of a synthetic hyperfine lattice. The gain is provided by evaporative cooling of appropriately chosen initial thermal atoms. We couple ground state hyperfine levels of <sup>87</sup>Rb atoms by microwaves to realize a lattice along a synthetic dimension made of hyperfine states<sup>45–49</sup>. We show that a BEC can be formed in a dark state of a three-site lattice by preparing thermal atoms, using Stimulated Raman Adiabatic Passage (STIRAP)<sup>50,51</sup>, in the coherent superposition of two sites which form the dark state. Note that the concept of a dark state is crucially important for novel phenomena in quantum optics like electromagnetically induced transparency<sup>52</sup>, lasing without inversion<sup>53,54</sup>, and also plays an essential role in realizing a localized state in a flat-band in condensed matter systems<sup>55</sup> and a novel phenomenon of spatial adiabatic passage in matter-wave optics<sup>56</sup>. We furthermore realize a five-site Su-Schrieffer-Heeger chain and realize the formation of a BEC in its topological edge state. Formation of a BEC in an atomic gas has a close analogy to laser oscillation and sometimes referred to as atom laser<sup>57</sup>. We have thus demonstrated

lasing of atomic matter wave in a topological edge state, namely a topological atom laser. Our results make ultracold atomic gases a promising platform to study non-Hermitian quantum mechanics with both gain and loss, opening an avenue toward controlled study of topological atom optics and quantum many-body physics in non-Hermitian setups.

## RESULTS

We achieve gain engineering in a lattice made of a synthetic dimension using ground-state hyperfine sublevels of  $^{87}\text{Rb}$ . Here, we utilize long-lived nature of the  $^{87}\text{Rb}$  hyperfine states in the electronic ground state to observe the formation of a BEC in the synthetic lattice. By coupling hyperfine sublevels  $|F(=1,2), m_F\rangle$  in the ground  $5s^2S_{1/2}$  state of  $^{87}\text{Rb}$  with microwaves, we prepare 3-site and 5-site lattices in synthetic dimension, as shown in Fig. 1 a.

Our experiments start with  $^{87}\text{Rb}$  atoms above the critical temperature  $T_c$  for BEC trapped in the crossed optical dipole trap at about  $1064\text{ nm}^{58}$ . The subsequent microwave sequence consists of two stages: First, we apply time-dependent microwaves to prepare thermal atoms in a superposition of the synthetic lattice sites close to one edge. Then, further evaporative cooling is performed with microwave couplings kept constant (see Fig. 1 b). Resulting formation of a BEC corresponds to “lasing” of atoms at a specific eigenmode in the lattice. We properly choose initial thermal atoms so that the resulting BEC is formed not at the lowest-energy mode or a single hyperfine state but rather at an excited mode made of a coherent superposition of multiple hyperfine states.

The resulting site distributions are measured by applying Stern-Gerlach separation immediately after switching off the trap, as shown in Fig. 1 c.

We first perform an experiment with a 3-site lattice to demonstrate our ability to control the formation of BEC into a dark state, which is not the ground state of the 3-site lattice. Here, we exploit  $\lambda$ -type coupling scheme with temporal evolution known as STIRAP. Three levels  $|1,1\rangle$ ,  $|2,0\rangle$  and  $|1,-1\rangle$  are coupled by microwaves and construct a 3-site synthetic lattice (site 4, 3 and 2). The site indices are labeled to be consistent with the 5-site lattice we introduce later. The Hamiltonian in the rotating frame, in the matrix form, is

$$\mathcal{H} = \frac{\hbar}{2} \begin{pmatrix} 2\delta & \Omega_1 & 0 \\ \Omega_1 & 0 & \Omega_2 \\ 0 & \Omega_2 & -2\delta \end{pmatrix} \quad (1)$$

where  $\Omega_1$ ,  $\Omega_2$  are the Rabi frequencies of microwave couplings and  $\delta$  is the detuning due to a magnetic field fluctuation. If the two-photon resonance  $\delta = 0$  holds, a dark state, given by  $\cos\theta|1,1\rangle + \sin\theta|1,-1\rangle$  with  $\tan\theta = \Omega_1/\Omega_2$ , becomes one of the eigenstates of Eq.

1. By applying two microwaves in counter-intuitive order so that  $\theta$  changes from 0 to  $\pi/2$ , the dark state can adiabatically evolve from  $|1,1\rangle$  (site 4) into  $|1,-1\rangle$  (site 2). This process is well-known as STIRAP. We utilize this STIRAP process to prepare thermal atoms in a coherent superposition of synthetic lattice sites. Initially atoms are evaporatively cooled in the state  $|1,1\rangle$  (site 4). At  $T/T_c \sim 1.1$ , evaporation is paused and the STIRAP sequence is applied. The STIRAP with full sweep ( $\theta = 0 \rightarrow \pi/2$ ) takes  $\tau_{\text{full}} = 10\text{ ms}$ . In our experiment the final value of  $\theta$  is controlled by the actual sweep time  $\tau$ : e.g.,  $\tau/\tau_{\text{full}} = 0.5$  leads to the equal superposition of site 4 and 2. After the sweep, we keep the microwave coupling and restart evaporation to form BEC, followed by the site occupation measurement. As we will show, the BEC is predominantly formed in the dark state where the thermal atoms are prepared.

Figure 2 shows the site occupancies  $N_4$ ,  $N_3$  and  $N_2$  as well as the number of Bose-condensed atoms  $N_{4c}$ ,  $N_{3c}$ , and  $N_{2c}$ , measured at three different  $t = \tau/\tau_{\text{full}}$  (see Extended Data Table I). Figure 2a shows the early stage  $t = 0.3$  where atoms almost localize in the site 4. By choosing different values of  $t$ , the atoms can be transferred to the site 2 (Fig. 2c) or in between the two sites as in Fig. 2b. The success of the “STIRAP” between the sites 4 and 2 indicates the coherent superposition is maintained during the process. In the third (fourth) row of Fig. 2, we plot the number of atoms (Bose-condensed atoms) in sites 4 versus site 2 normalized by the total number of atoms (Bose-condensed atoms) for each performed experiment. Although there is large fluctuation in the value of  $N_2$  and  $N_4$  ( $N_{2c}$  and  $N_{4c}$ ), the experimental results lie along the line  $N_4 + N_2 = N$  and  $N_{4c} + N_{2c} = N_c$ . Here,  $N$  is the total number of observed atoms, and  $N_c$  is the total number of atoms in the condensate. The absence of particles in the intermediate state  $N_3$  is the indication that the atoms are in the dark state. Small but nonzero  $N_3$  is caused by the deviation of the microwave frequencies from the resonances.

We note that the dark state where the condensate is formed is not the ground state of the lattice. This formation of BEC at an excited state can be understood by the difference of the critical temperatures; among the three dressed states, the dark state had most thermal atoms and thus has the highest BEC transition temperature, resulting in preferred formation of the BEC. We can alternatively describe this process in terms of different effective gain for each lattice site. Although evaporative cooling acts on all sites equally, the initial nonequal distribution of thermal atoms results in different effective gain for each site. Sites with more thermal atoms imply larger effective gain, and since the thermal atoms are initially distributed to the sites forming the dark state, the preferred lasing, namely BEC, takes place at the dark state. In our system, the stability of the state transfer is limited by the existence of a magnetic field fluctua-

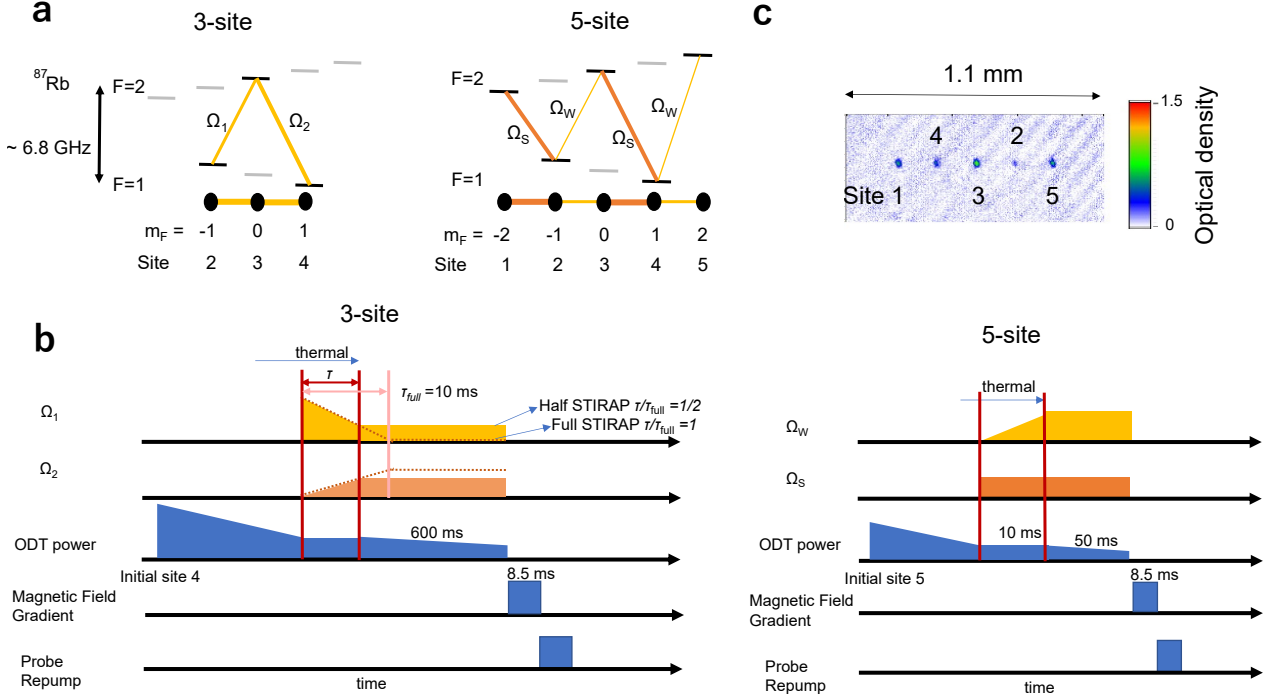


FIG. 1: **Schematic of the experiment.** **a**, microwave coupling scheme. The 3-site lattice with  $\Lambda$ -type coupling (left) and the 5-site lattice with  $W$ -type coupling (right) are shown. Rabi frequencies for the microwave coupling are indicated by  $\Omega_i (i = 1, 2, W, S)$ . Each state is named as site1-5 of the synthetic lattice. **b**, Experimental sequence. For both 3- and 5-site experiments, thermal atoms are loaded with microwaves of varying Rabi frequencies to create a superposition and then cooled to achieve BEC. The 3-site sequence is parameterized by  $\tau/\tau_{full}$  where  $\tau_{full}$  is the time required for STIRAP is accomplished. At the time  $\tau$  after the microwave sequence starts, Rabi frequencies are kept constant and atoms with superposition are cooled to BEC. Similarly, the 5-site sequence is characterized by the final ratio of  $\Omega_W/\Omega_S$ .  $\Omega_i (i = W, S)$  is defined as averaged Rabi frequencies of the same kind of microwaves. **c**, Site-resolved imaging by Stern-Gerlach separation. The image is taken after 8.5ms of free expansion.

tion and the uncertainty in determining microwave resonances. Both of them can cause a two-photon detuning of the  $\Lambda$ -transition, which eliminates the dark state. See Methods for the stabilization of the magnetic field. We note that formation of BEC in a dark state of momentum states was recently reported in Ref.<sup>59</sup> through a kind of mode-conversion by coupling atoms already in a BEC to an optical cavity. Our approach, instead, provides a direct means to control gain in ultracold atomic setups.

Next we realize a 5-sites Su-Schrieffer-Heeger (SSH) lattice<sup>60</sup> to obtain the topological edge-state lasing, or the topological atom laser. The SSH model is a one-dimensional lattice model with alternating hopping strengths, whose Hamiltonian in the rotating frame is

$$H_{SSH} = \hbar \left( \frac{\Omega_A}{2} \sum_i |2i\rangle \langle 2i-1| + \frac{\Omega_B}{2} \sum_i |2i+1\rangle \langle 2i| \right) + \text{H.c.}, \quad (2)$$

where the sum of  $i$  runs over integer values. The energy bandgap closes at  $\Omega_A = \Omega_B$ , and the regions  $\Omega_A > \Omega_B$

and  $\Omega_A < \Omega_B$  are topologically distinct. Due to the bulk-edge correspondence, when a lattice is terminated at  $i = 1$  by restricting the above sum to  $i \geq 1$ , there exists a zero-energy edge state localized around the edge if and only if  $\Omega_A < \Omega_B$ , and this zero-energy state has non-zero amplitude only on odd sites  $(1, 3, 5, \dots)$ . The existence of the zero-energy edge-localized state is topologically robust; small spatial inhomogeneity in  $\Omega_A$  and  $\Omega_B$  will not destroy the edge state. As we see, such inhomogeneity is naturally present in our setup and thus the topological atom laser we realize is directly benefited from the topological robustness.

In our experiment, five levels  $|2, -2\rangle$ ,  $|1, -1\rangle$ ,  $|2, 0\rangle$ ,  $|1, 1\rangle$  and  $|2, 2\rangle$  are coupled by microwaves and construct a 5-site synthetic lattice (site 1-5, respectively) for which the Hamiltonian in the rotating frame can be written in

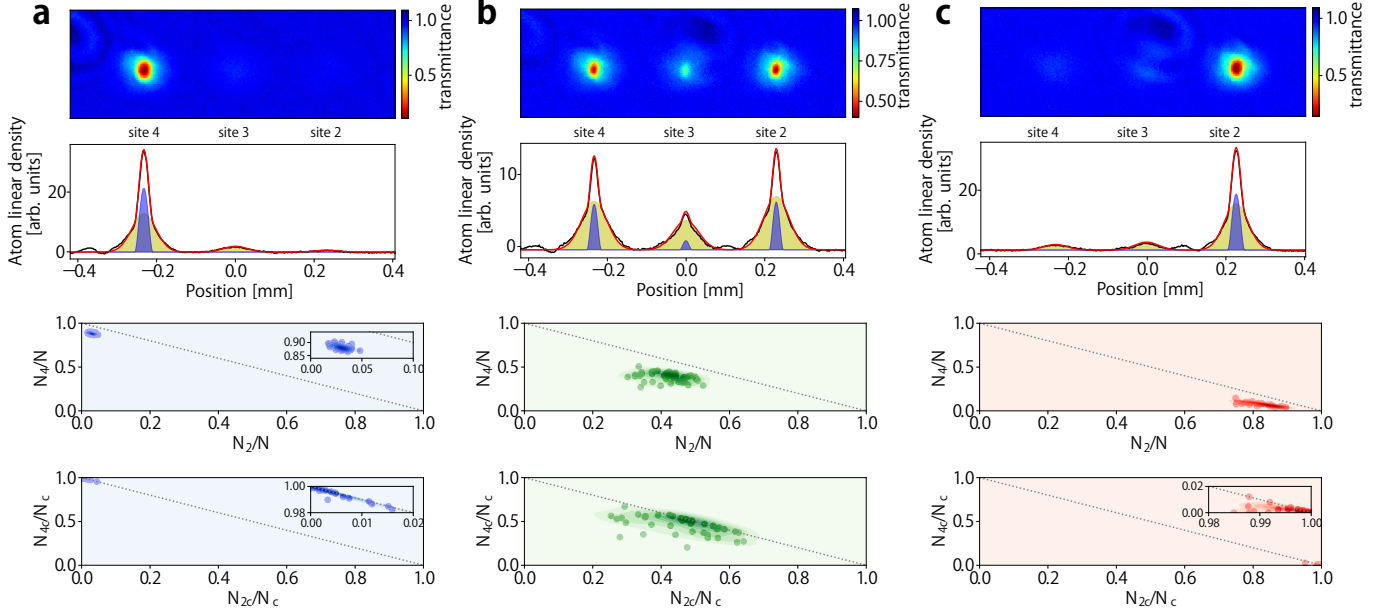


FIG. 2: **Gain engineering in the 3-site synthetic lattice.** Site distributions after the 3-site sequence with **a**,  $\tau/\tau_{full} = 0.3$  **b**  $\tau/\tau_{full} = 0.5$  **c**  $\tau/\tau_{full} = 0.8$ . The top figures are typical site-resolved images (time of flight is 8.5 ms) together with the corresponding column densities (black lines) with the results of bimodal fitting (red lines), where thermal and BEC components are indicated by the yellow and blue shaded area, respectively. The lower graphs are statistical distributions taken over at least 30 experimental runs.  $N_i$  ( $N_{ic}$ ) indicates the total (condensate) atom number in the site  $i$  and  $N_c = \sum_i N_{ic}$ . The blue dotted line in the scatter diagrams indicates the trajectory for the ideal dark state  $N_3 = 0$  ( $N_{3c} = 0$ ), and the shading visualizes statistical distribution of experimental results.

the matrix form

$$\mathcal{H} = \frac{\hbar}{2} \begin{pmatrix} -4\delta & \Omega_S^{(1)} & 0 & 0 & 0 \\ \Omega_S^{(1)} & 2\delta & \Omega_W^{(1)} & 0 & 0 \\ 0 & \Omega_W^{(1)} & 0 & \Omega_S^{(2)} & 0 \\ 0 & 0 & \Omega_S^{(2)} & -2\delta & \Omega_W^{(2)} \\ 0 & 0 & 0 & \Omega_W^{(2)} & 4\delta \end{pmatrix} \quad (3)$$

where  $\Omega_W^{(1,2)}$  and  $\Omega_S^{(1,2)}$  are the Rabi frequencies in microwave couplings, and  $\delta$  is the detuning due to a magnetic field fluctuation. The ideal SSH model is obtained if  $\Omega_i^{(1)} = \Omega_i^{(2)}$  for  $i = S, W$ , and the edge state localized around site 5 exists when  $\Omega_W < \Omega_S$ ; such an edge state is a superposition of only three sites, (sites 5, 3 and 1) if  $\delta=0$ . In our setup,  $\Omega_i^{(1)}$  and  $\Omega_i^{(2)}$  are not exactly equal because of the different Clebsch-Gordan coefficients. As we noted above, the existence of a topological edge state is robust against such inhomogeneity or disorder in hopping amplitudes. Below we use the averaged values  $\langle \Omega_i \rangle = (\Omega_i^{(1)} + \Omega_i^{(2)})/2$  for these couplings to characterize the strong and weak couplings. (See Extended Data Table II and Extended Data Fig. 2 for more details).

To achieve BEC in the topological edge state, thermal atoms initially populated in the site 4 are first transferred

to the site 5 by adiabatic rapid passage. Four microwaves  $\Omega_W^{(1,2)}, \Omega_S^{(1,2)}$  are then applied as shown in Fig. 1 a. Thermal atoms will then adiabatically populate the topological edge mode extending over sites 5, 3, and 1. Finally, we keep the microwave coupling and restart evaporation to accomplish BEC, followed by the site occupation measurement. We performed experiments with four values of the final ratios  $r = \langle \Omega_W \rangle / \langle \Omega_S \rangle (< 1)$  to confirm the behavior of the topological edge-state lasing.

Figure 3(a-c) shows that the TOF signals after the Stern-Gerlach separation, revealing site occupancies  $N_i$  ( $i = 1, \dots, 5$ ) at three different values of  $r$ . We note that as in Fig. 1 c, the top two rows of Fig. 3 showing site occupancy is ordered in sites 1, 4, 3, 2, 5, which is not a simple ascending order. We see that in all three values of  $r$ , the BEC phase transition, namely, atom lasing is successfully observed, and the formed BEC has the largest population in site 5, with decreasing atom numbers in 3 and 1 with almost no occupation in 2 and 4, which is consistent with the wavefunction profile of the topological edge state of the SSH model (See Extended Data Fig. 2). In the bottom two rows of Fig. 3, we plot  $N_5$  ( $N_{5c}$ ) versus  $N_1 + N_3$  ( $N_{1c} + N_{3c}$ ). The alignment of the data along the line  $N_5 + N_3 + N_1 = N$  and  $N_{5c} + N_{3c} + N_{1c} = N_c$  indicate that the population in sites 2 and 4 are small

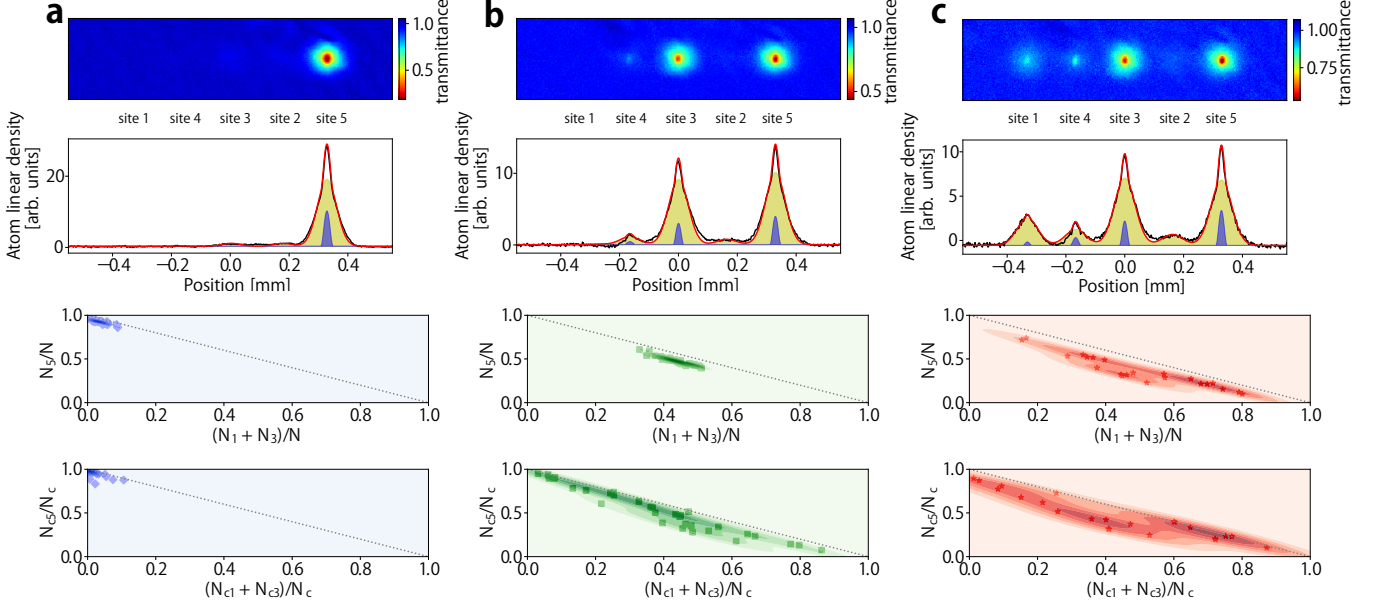


FIG. 3: **Gain engineering for topological edge states in the 5-site SSH model.** The data taken at **a**  $r = \langle \Omega_W \rangle / \langle \Omega_S \rangle = 0.097$ , **b**  $r = 0.23$  and **c**  $r = 0.45$  are shown. From top to bottom, the figures are typical imaging (time of flight is 8.5 ms), the corresponding column density with the best fit bimodal function, and the site distribution statistics for both total and condensate atom numbers, as introduced in Fig. 2. The blue dotted line in the scatter diagram means the trajectory of the ideal edge state ( $N_2 + N_4 = 0$ ,  $N_{2c} + N_{4c} = 0$ ), and shading visualizes statistical distribution of experimental result.

as expected; we give more detailed explanation on this point in Discussions below.

We have moreover performed an additional experiment to confirm coherence of this superposition as shown in Fig. 4. After loading atoms into the lattice with largest  $r$ , we apply the reverse process back to the  $r = 0$ . The resulting site population returns to the initial site 5, proving that the coherence persisted throughout the entire process; the system keeps adiabaticity even in the presence of random fluctuations in  $\delta$ .

## DISCUSSIONS

Although the lower two panels in Fig. 3 confirm that the population mainly evolves along the line  $N_1 + N_3 + N_5 = 1$ , we should mention that there is non-negligible occupancy of site 4 in Fig. 3c. The site 4 is in between largely populated sites 5 and 3, and even a little fluctuation in  $\delta$  can result in occupation of site 4. Large fluctuations seen in the site occupation of BEC comes from the small BEC fraction: for the 5-site experiment the state mainly populates the upper hyperfine levels which suffer from inelastic collisions. However, the most probable site distribution for each coupling strength is consistent with the theoretical prediction ( $(N_5, N_1 + N_3) = (0.98, 0.02)$ ,  $(0.66, 0.34)$  and  $(0.26, 0.74)$  for  $r = 0.097, 0.23, 0.45$ , re-

spectively).

One of the characteristics of topological systems is robustness to external disturbances. Indeed, the topological atom laser is realized despite the natural inhomogeneity or disorder in the coupling,  $\Omega_S^{(1)} \neq \Omega_S^{(2)}$  and  $\Omega_W^{(1)} \neq \Omega_W^{(2)}$ . We should also note that the zero energy topological edge state is not robust against onsite disorders, namely again nonzero  $\delta$ . The existence of nonzero population in sites 2 and 4 seen in the experiment is ascribed to nonzero  $\delta$ . Even though the onsite disorder makes the energy of the edge state to become nonzero, the edge localized mode can still persist as long as the effect of  $\delta$  is smaller than the band gap,  $2(\Omega_S - \Omega_W)$ , which is the case in our experiment.

## CONCLUSION AND PROSPECTS

By preparing the initial thermal atoms in a proper dressed state of the synthetic lattice, we observe the formation of BEC in the dressed state even when the dressed state is not the ground state of the lattice. Such a formation of BEC in a dressed mode can be regarded as laser oscillation of an atomic matter wave. In particular, the 5-site experiment demonstrates topological atom laser oscillating at the topological edge state. The cur-

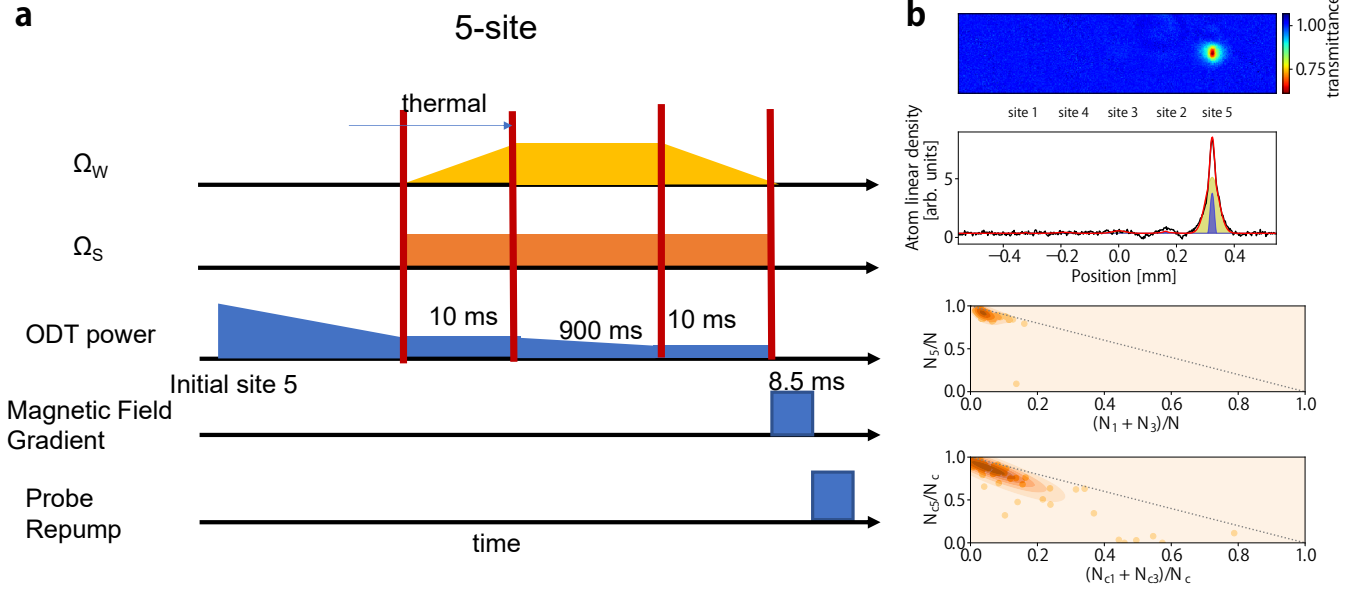


FIG. 4: **Confirmation of coherence of superposition on the BEC in the edge state.** **a**, experimental sequence. For 5-site reverse experiments. **b**, the data taken at  $r = 0$  after reversed process from  $r = 0.45$  are shown. The figures from top to bottom respectively correspond to typical imaging (time of flight is 8.5ms), the corresponding column density with the best fit bimodal function, and the site distribution statistics for both total and condensate atom numbers, as introduced in Fig. 3.

rent limitation is the external field fluctuations which can be improved by appropriate shielding and active stabilization<sup>61–63</sup>. Increasing Rabi frequencies and shortening the experimental time scale will help reducing the effect of both field fluctuations and inelastic loss.

Our results successfully demonstrate that an effective site-dependent gain can be engineered through evaporative cooling by appropriate preparation of the initial thermal state. Such a gain-loss control in ultracold atomic gases provide a versatile tool to study non-Hermitian physics. Combining with the ability to control losses and inter-particle interactions, one can now explore much broader classes of non-Hermitian quantum many-body physics in ultracold atomic gases. Our results also show that atom optics can be combined with concepts developed in topological photonics, opening the field of topological atom optics. This work thus serves as the next footstep to further studies and applications of topological and/or non-Hermitian physics.

#### DATA AVAILABILITY

All the data presented in this paper are available from the corresponding author upon reasonable request.

#### CODE AVAILABILITY

The computational codes used for the analysis of the experimental data are available from the corresponding author upon reasonable request.

#### REFERENCE

- 
- \* Electronic address: taie@scphys.kyoto-u.ac.jp
- [1] Acín, A. *et al.* The quantum technologies roadmap: a european community view. *New Journal of Physics* **20**, 080201 (2018). URL <https://iopscience.iop.org/article/10.1088/1367-2630/aad1ea>.
  - [2] Moiseyev, N. *Non-Hermitian quantum mechanics* (Cambridge University Press, 2011). URL <https://www.cambridge.org/core/books/nonhermitian-quantum-mechanics/134430A6587FF19542FD4A47325BF60E>.
  - [3] Ashida, Y., Gong, Z. & Ueda, M. Non-hermitian physics. *Advances in Physics* **69**, 249–435 (2020). URL <https://www.tandfonline.com/doi/abs/10.1080/00018732.2021.1876991>.
  - [4] Gamow, G. Zur quantentheorie des atomkernes. *Zeitschrift für Physik* **51**, 204–212 (1928). URL <https://link.springer.com/article/10.1007/BF01343196>.



- [5] Bender, C. M. & Boettcher, S. Real spectra in non-hermitian hamiltonians having  $\mathcal{PT}$  symmetry. *Phys. Rev. Lett.* **80**, 5243–5246 (1998). URL <https://link.aps.org/doi/10.1103/PhysRevLett.80.5243>.
- [6] Bender, C. M. Making sense of non-hermitian hamiltonians. *Reports on Progress in Physics* **70**, 947 (2007). URL <https://iopscience.iop.org/article/10.1088/0034-4885/70/6/R03>.
- [7] Bergholtz, E. J., Budich, J. C. & Kunst, F. K. Exceptional topology of non-hermitian systems. *Rev. Mod. Phys.* **93**, 015005 (2021). URL <https://link.aps.org/doi/10.1103/RevModPhys.93.015005>.
- [8] Okuma, N. & Sato, M. Non-hermitian topological phenomena: A review. *Annual Review of Condensed Matter Physics* **14**, 83–107 (2023).
- [9] St-Jean, P. *et al.* Lasing in topological edge states of a one-dimensional lattice. *Nature Photonics* **11**, 651–656 (2017). URL <https://www.nature.com/articles/s41566-017-0006-2>.
- [10] Parto, M. *et al.* Edge-mode lasing in 1d topological active arrays. *Phys. Rev. Lett.* **120**, 113901 (2018). URL <https://link.aps.org/doi/10.1103/PhysRevLett.120.113901>.
- [11] Zhao, H. *et al.* Topological hybrid silicon microlasers. *Nature communications* **9**, 981 (2018). URL <https://www.nature.com/articles/s41467-018-03434-2>.
- [12] Ota, Y., Katsumi, R., Watanabe, K., Iwamoto, S. & Arakawa, Y. Topological photonic crystal nanocavity laser. *Communications Physics* **1**, 86 (2018). URL <https://www.nature.com/articles/s42005-018-0083-7>.
- [13] Bahari, B. *et al.* Nonreciprocal lasing in topological cavities of arbitrary geometries. *Science* **358**, 636–640 (2017). URL <https://www.science.org/doi/10.1126/science.aao4551>.
- [14] Bandres, M. A. *et al.* Topological insulator laser: Experiments. *Science* **359**, eaar4005 (2018). URL <https://www.science.org/doi/10.1126/science.aar4005>.
- [15] Klemmt, S. *et al.* Exciton-polariton topological insulator. *Nature* **562**, 552–556 (2018). URL <https://www.nature.com/articles/s41586-018-0601-5>.
- [16] Price, H. *et al.* Roadmap on topological photonics. *Journal of Physics: Photonics* **4**, 032501 (2022). URL <https://iopscience.iop.org/article/10.1088/2515-7647/ac4ee4>.
- [17] Dalibard, J., Castin, Y. & Mølmer, K. Wave-function approach to dissipative processes in quantum optics. *Phys. Rev. Lett.* **68**, 580–583 (1992). URL <https://link.aps.org/doi/10.1103/PhysRevLett.68.580>.
- [18] Daley, A. J. Quantum trajectories and open many-body quantum systems. *Advances in Physics* **63**, 77–149 (2014). URL <https://www.tandfonline.com/doi/full/10.1080/00018732.2014.933502>.
- [19] Lee, T. E. & Chan, C.-K. Heralded magnetism in non-hermitian atomic systems. *Phys. Rev. X* **4**, 041001 (2014). URL <https://link.aps.org/doi/10.1103/PhysRevX.4.041001>.
- [20] San-Jose, P., Cayao, J., Prada, E. & Aguado, R. Majorana bound states from exceptional points in non-topological superconductors. *Scientific reports* **6**, 21427 (2016). URL <https://www.nature.com/articles/srep21427>.
- [21] Lourenço, J. A. S., Eneias, R. L. & Pereira, R. G. Kondo effect in a  $\mathcal{PT}$ -symmetric non-hermitian hamiltonian. *Phys. Rev. B* **98**, 085126 (2018). URL <https://link.aps.org/doi/10.1103/PhysRevB.98.085126>.
- [22] Nakagawa, M., Kawakami, N. & Ueda, M. Non-hermitian kondo effect in ultracold alkaline-earth atoms. *Phys. Rev. Lett.* **121**, 203001 (2018). URL <https://link.aps.org/doi/10.1103/PhysRevLett.121.203001>.
- [23] Ghatak, A. & Das, T. Theory of superconductivity with non-hermitian and parity-time reversal symmetric cooper pairing symmetry. *Phys. Rev. B* **97**, 014512 (2018). URL <https://link.aps.org/doi/10.1103/PhysRevB.97.014512>.
- [24] Yamamoto, K. *et al.* Theory of non-hermitian fermionic superfluidity with a complex-valued interaction. *Phys. Rev. Lett.* **123**, 123601 (2019). URL <https://link.aps.org/doi/10.1103/PhysRevLett.123.123601>.
- [25] Hamazaki, R., Kawabata, K. & Ueda, M. Non-hermitian many-body localization. *Phys. Rev. Lett.* **123**, 090603 (2019). URL <https://link.aps.org/doi/10.1103/PhysRevLett.123.090603>.
- [26] Yoshida, T., Kudo, K. & Hatsugai, Y. Non-hermitian fractional quantum hall states. *Scientific reports* **9**, 16895 (2019). URL <https://www.nature.com/articles/s41598-019-53253-8>.
- [27] Lee, E., Lee, H. & Yang, B.-J. Many-body approach to non-hermitian physics in fermionic systems. *Phys. Rev. B* **101**, 121109 (2020). URL <https://link.aps.org/doi/10.1103/PhysRevB.101.121109>.
- [28] Guo, C.-X., Wang, X.-R., Wang, C. & Kou, S.-P. Non-hermitian dynamic strings and anomalous topological degeneracy on a non-hermitian toric-code model with parity-time symmetry. *Phys. Rev. B* **101**, 144439 (2020). URL <https://link.aps.org/doi/10.1103/PhysRevB.101.144439>.
- [29] Matsumoto, N., Kawabata, K., Ashida, Y., Furukawa, S. & Ueda, M. Continuous phase transition without gap closing in non-hermitian quantum many-body systems. *Phys. Rev. Lett.* **125**, 260601 (2020). URL <https://link.aps.org/doi/10.1103/PhysRevLett.125.260601>.
- [30] Liu, T., He, J. J., Yoshida, T., Xiang, Z.-L. & Nori, F. Non-hermitian topological mott insulators in one-dimensional fermionic superlattices. *Phys. Rev. B* **102**, 235151 (2020). URL <https://link.aps.org/doi/10.1103/PhysRevB.102.235151>.
- [31] Mu, S., Lee, C. H., Li, L. & Gong, J. Emergent fermi surface in a many-body non-hermitian fermionic chain. *Phys. Rev. B* **102**, 081115 (2020). URL <https://link.aps.org/doi/10.1103/PhysRevB.102.081115>.
- [32] Hayata, T. & Yamamoto, A. Non-hermitian hubbard model without the sign problem. *Phys. Rev. B* **104**, 125102 (2021). URL <https://link.aps.org/doi/10.1103/PhysRevB.104.125102>.
- [33] Gopalakrishnan, S. & Gullans, M. J. Entanglement and purification transitions in non-hermitian quantum mechanics. *Phys. Rev. Lett.* **126**, 170503 (2021). URL <https://link.aps.org/doi/10.1103/PhysRevLett.126.170503>.
- [34] Makris, K. G., El-Ganainy, R., Christodoulides, D. N. & Musslimani, Z. H. Beam dynamics in  $\mathcal{PT}$  symmetric optical lattices. *Phys. Rev. Lett.* **100**, 103904 (2008). URL <https://link.aps.org/doi/10.1103/PhysRevLett.100.103904>.
- [35] Guo, A. *et al.* Observation of  $\mathcal{PT}$ -symmetry breaking in complex optical potentials. *Phys. Rev. Lett.* **103**, 093902 (2009). URL <https://link.aps.org/doi/10.1103/PhysRevLett.103.093902>.

- 1103/PhysRevLett.103.093902.
- [36] Rüter, C. E. *et al.* Observation of parity–time symmetry in optics. *Nature physics* **6**, 192–195 (2010). URL <https://www.nature.com/articles/nphys1515>.
  - [37] Konotop, V. V., Yang, J. & Zezyulin, D. A. Nonlinear waves in  $\mathcal{PT}$ -symmetric systems. *Rev. Mod. Phys.* **88**, 035002 (2016). URL <https://link.aps.org/doi/10.1103/RevModPhys.88.035002>.
  - [38] Longhi, S. Parity-time symmetry meets photonics: A new twist in non-hermitian optics. *Europhysics Letters* **120**, 64001 (2018). URL <https://iopscience.iop.org/article/10.1209/0295-5075/120/64001>.
  - [39] El-Ganainy, R., Khajavikhan, M., Christodoulides, D. N. & Ozdemir, S. K. The dawn of non-hermitian optics. *Communications Physics* **2**, 37 (2019). URL <https://www.nature.com/articles/s42005-019-0130-z>.
  - [40] Bloch, I., Dalibard, J. & Zwerger, W. Many-body physics with ultracold gases. *Rev. Mod. Phys.* **80**, 885–964 (2008). URL <https://link.aps.org/doi/10.1103/RevModPhys.80.885>.
  - [41] Bloch, I., Dalibard, J. & Nascimbene, S. Quantum simulations with ultracold quantum gases. *Nature Physics* **8**, 267–276 (2012). URL <https://www.nature.com/articles/nphys2259>.
  - [42] Schäfer, F., Fukuhara, T., Sugawa, S., Takasu, Y. & Takahashi, Y. Tools for quantum simulation with ultracold atoms in optical lattices. *Nature Reviews Physics* **2**, 411–425 (2020). URL <https://www.nature.com/articles/s42254-020-0195-3>.
  - [43] Takasu, Y. *et al.*  $\mathcal{PT}$ -symmetric non-hermitian quantum many-body system using ultracold atoms in an optical lattice with controlled dissipation. *Progress of Theoretical and Experimental Physics* **2020**, 12A110 (2020). URL <https://academic.oup.com/ptep/article/2020/12/12A110/5905047>.
  - [44] Ren, Z. *et al.* Chiral control of quantum states in non-hermitian spin–orbit-coupled fermions. *Nature Physics* **18**, 385–389 (2022). URL <https://www.nature.com/articles/s41567-021-01491-x>.
  - [45] Boada, O., Celi, A., Latorre, J. I. & Lewenstein, M. Quantum Simulation of an Extra Dimension. *Physical Review Letters* **108**, 133001 (2012). URL <https://link.aps.org/doi/10.1103/PhysRevLett.108.133001>.
  - [46] Celi, A. *et al.* Synthetic Gauge Fields in Synthetic Dimensions. *Physical Review Letters* **112**, 043001 (2014). URL <https://link.aps.org/doi/10.1103/PhysRevLett.112.043001>.
  - [47] Mancini, M. *et al.* Observation of chiral edge states with neutral fermions in synthetic Hall ribbons. *Science* **349**, 1510–1513 (2015). URL <https://science.sciencemag.org/content/349/6255/1510>. Publisher: American Association for the Advancement of Science Section: Report.
  - [48] Stuhl, B. K., Lu, H.-I., Aycock, L. M., Genkina, D. & Spielman, I. B. Visualizing edge states with an atomic Bose gas in the quantum Hall regime. *Science* **349**, 1514–1518 (2015). URL <https://www.science.org/doi/10.1126/science.aaa8515>.
  - [49] Ozawa, T. & Price, H. M. Topological quantum matter in synthetic dimensions. *Nature Reviews Physics* **1**, 349–357 (2019). URL <https://www.nature.com/articles/s42254-019-0045-3>. Number: 5 Publisher: Nature Publishing Group.
  - [50] Kuklinski, J. R., Gaubatz, U., Hioe, F. T. & Bergmann, K. Adiabatic population transfer in a three-level system driven by delayed laser pulses. *Physical Review A* **40**, 6741–6744 (1989). URL <https://link.aps.org/doi/10.1103/PhysRevA.40.6741>.
  - [51] Bergmann, K., Theuer, H. & Shore, B. W. Coherent population transfer among quantum states of atoms and molecules. *Reviews of Modern Physics* **70**, 1003–1025 (1998). URL <https://link.aps.org/doi/10.1103/RevModPhys.70.1003>.
  - [52] Fleischhauer, M., Imamoglu, A. & Marangos, J. P. Electromagnetically induced transparency: Optics in coherent media. *Rev. Mod. Phys.* **77**, 633–673 (2005). URL <https://link.aps.org/doi/10.1103/RevModPhys.77.633>.
  - [53] Scully, M. O., Zhu, S.-Y. & Gavrielides, A. Degenerate quantum-beat laser: Lasing without inversion and inversion without lasing. *Phys. Rev. Lett.* **62**, 2813–2816 (1989). URL <https://link.aps.org/doi/10.1103/PhysRevLett.62.2813>.
  - [54] Mompert, J. & Corbalán, R. Lasing without inversion. *Journal of Optics B: Quantum and Semiclassical Optics* **2**, R7 (2000). URL <https://dx.doi.org/10.1088/1464-4266/2/3/201>.
  - [55] Taie, S. *et al.* Coherent driving and freezing of bosonic matter wave in an optical lieb lattice. *Science Advances* **1**, e1500854 (2015). URL <https://www.science.org/doi/abs/10.1126/sciadv.1500854>. <https://www.science.org/doi/pdf/10.1126/sciadv.1500854>.
  - [56] Taie, S., Ichinose, T., Ozawa, H. & Takahashi, Y. Spatial adiabatic passage of massive quantum particles in an optical Lieb lattice. *Nature Communications* **11**, 257 (2020).
  - [57] Robins, N., Altin, P., Debs, J. & Close, J. Atom lasers: Production, properties and prospects for precision inertial measurement. *Physics Reports* **529**, 265–296 (2013). URL <https://linkinghub.elsevier.com/retrieve/pii/S037015731300118X>.
  - [58] Huang, C.-Y. *et al.* A simple recipe for rapid all-optical formation of spinor Bose-Einstein condensates. *Journal of Physics B: Atomic, Molecular and Optical Physics* **50**, 155302 (2017). URL <https://iopscience.iop.org/article/10.1088/1361-6455/aa7980>.
  - [59] Skulte, J. *et al.* Condensate Formation in a Dark State of a Driven Atom-Cavity System. *Physical Review Letters* **130**, 163603 (2023). URL <https://link.aps.org/doi/10.1103/PhysRevLett.130.163603>.
  - [60] Su, W. P., Schrieffer, J. R. & Heeger, A. J. Solitons in Polyacetylene. *Physical Review Letters* **42**, 1698–1701 (1979). URL <https://link.aps.org/doi/10.1103/PhysRevLett.42.1698>.
  - [61] Merkel, B. *et al.* Magnetic field stabilization system for atomic physics experiments. *Review of Scientific Instruments* **90**, 044702 (2019). URL <https://pubs.aip.org/aip/rsi/article/283219>.
  - [62] Xu, X.-T. *et al.* Ultra-low noise magnetic field for quantum gases. *Review of Scientific Instruments* **90**, 054708 (2019). URL <https://pubs.aip.org/aip/rsi/article/361080>.
  - [63] Borkowski, M. *et al.* Active stabilization of kilogauss magnetic fields to the ppm level for magnetooassociation on ultranarrow Feshbach resonances. *Review of Scientific Instruments* **94**, 073202 (2023). URL <https://pubs.aip.org/rsi/article/94/7/073202/2901328/>



Active-stabilization-of-kilogauss-magnetic-fields.

## METHODS

**Experimental setup** Our experiments start with  $^{87}\text{Rb}$  atoms above the critical temperature for Bose-Einstein condensation (BEC) trapped in the crossed optical dipole trap at about 1064 nm (see Extended Data Fig. 1). The crossing optical dipole trap is created with two horizontal beams which are crossing at slight angle to provide a large trap volume and a vertical beam (Extended Data Fig. 1). Then the  $^{87}\text{Rb}$  atoms are pumped to a hyperfine state  $|F=1, m_F=1\rangle$  of the  $^2\text{S}_{1/2}$  electronic ground state by optical pumping. For 5-site experiment, we further transfer atoms into the  $|F=2, m_F=2\rangle$  state by adiabatic rapid passage (ARP) with microwave irradiation. For efficient evaporative cooling, we turn off a deeper horizontal beam in the middle of evaporative cooling. In order to induce coupling between the hyperfine states, or neighboring sites in the synthetic dimension, we apply resonant microwave fields. The subsequent sequence of the microwave irradiation consists of two stages: First, we apply time-dependent microwaves to prepare thermal atoms in a desired superposition of the synthetic lattice sites. Then, further evaporative cooling is performed with microwave couplings kept constant. Resulting formation of a BEC can be regarded as “lasing” of atoms at a specific eigenmode in the lattice.

### Generation of 4-color microwave

We simultaneously apply 4-color microwaves around the clock frequency  $\sim 6.8\text{GHz}$ . We use an output from a microwave synthesizer at a frequency  $f$  for the  $|2, -2\rangle - |1, -1\rangle$  coupling and generate three sidebands. An image rejection mixer can create a microwave sideband only at higher frequency side at a frequency of  $f + f_{\text{RF1}}$ , and is set on resonance to the  $|2, 0\rangle - |1, 1\rangle$  transition. A series connection of an additional image rejection mixer further generates sidebands at  $f + f_{\text{RF2}}$  and  $f + f_{\text{RF1}} + f_{\text{RF2}}$ , and are set to the  $|2, 0\rangle - |1, -1\rangle$  and  $|2, 2\rangle - |1, 1\rangle$  resonances (Extended Data Fig. 3). In this configuration,  $\Omega_{\text{W}}$  can be controlled by the strength of the second RF.

**Suppression of magnetic field fluctuation** One of the major sources of the short-term magnetic field fluctuations comes from electric devices around the experimental chamber. Transducers in power supply emit strong noises at alternate current (AC) line frequency (60 Hz) and its harmonics which amounts to  $\sim 0.8$  mG at the chamber. We construct a feed-forward system to suppress the AC field fluctuation. We monitor field fluctuations by a flux gate sensor placed near the magnetic coil on the quantization axis. A function generator with

a reference clock of 10 MHz locked to the AC line (DS technology) generates 60 Hz harmonics up to 7th order to be added to the analog control of the coil. The amplitudes and phases of the harmonics is tuned to minimize the fluctuation of sensor output. This enables us to suppress the 60Hz line noise down to  $\sim 0.1$  mG at all times during the experiment.

## ACKNOWLEDGEMENTS

This work was supported by the Grant-in-Aid for Scientific Research of JSPS (No. JP17H06138, No. JP18H05405, No. JP18H05228, No. JP20H01845, No. JP21H01007 No. JP21H01014 and No. JP22K20356), JST CREST (Nos. JPMJCR1673, No. JPMJCR19T1 and JPMJCR23I3), JST PRESTO Grant No. JPMJPR2353, MEXT Quantum Leap Flagship Program (MEXT Q-LEAP) Grant No. JPMXS0118069021, and JST Moonshot R&D Grant No. JPMJMS2269.

## AUTHOR CONTRIBUTIONS

T. T. and S.T. carried out experiments. T. T. and Y. Takasu. analyzed the data. T. O. gave advice on experiments from the theoretical viewpoint. K. Y. contributed in the early stage of the experiment. Y. Takahashi conducted the whole experiment. All the authors contributed in discussing the result and writing the manuscript.

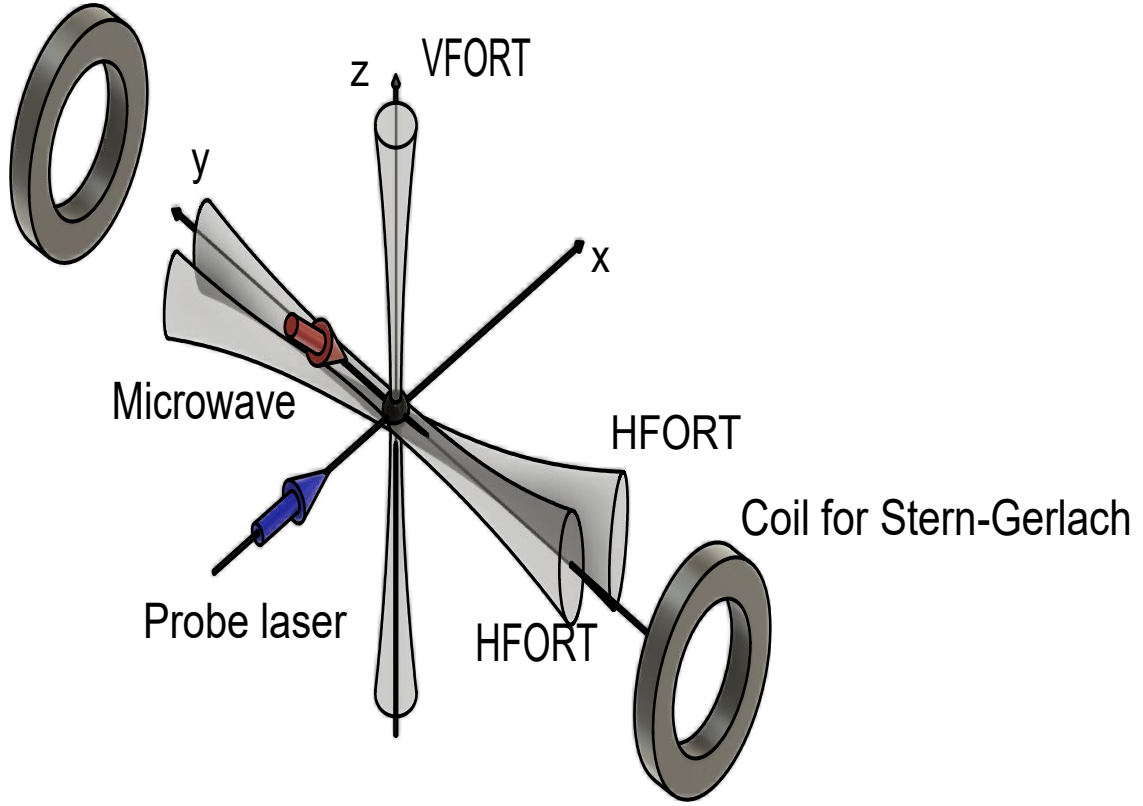
## COMPETING INTERESTS

The authors declare no competing interests.

## EXTENDED DATA

$\tau/\tau_{\text{full}}$ \backslash site	site 2 - 3 ( $\Omega_1/2\pi$ )	site 3 - 4 ( $\Omega_2/2\pi$ )
0.3	1.457	0.07560
0.4	1.376	0.2834
0.5	0.8410	0.6252
0.8	0.03283	1.144

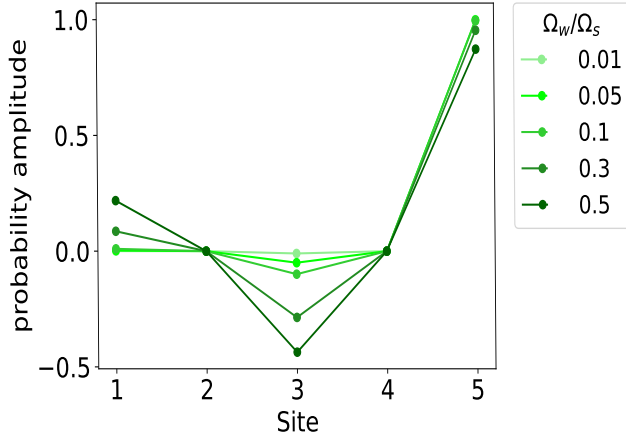
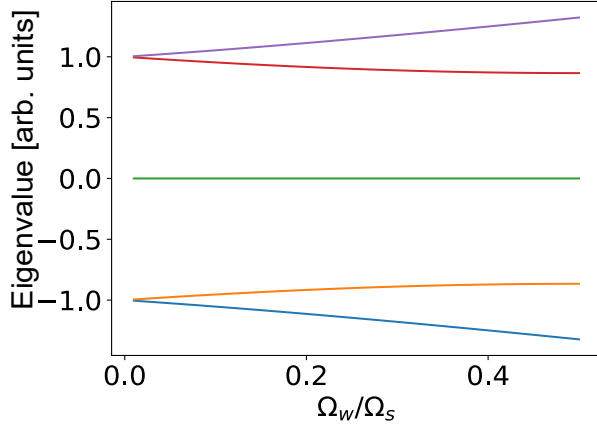
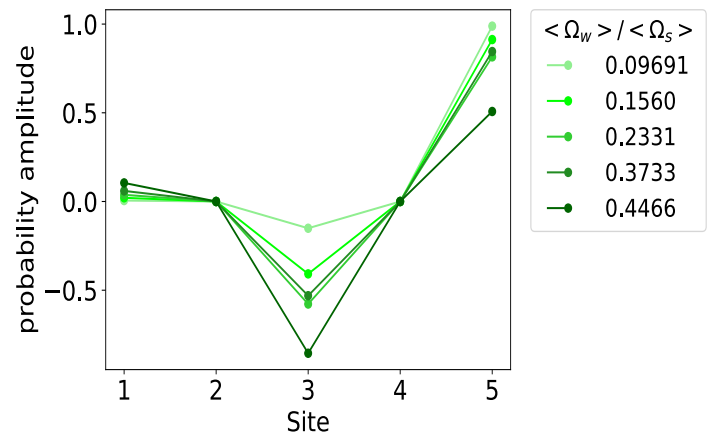
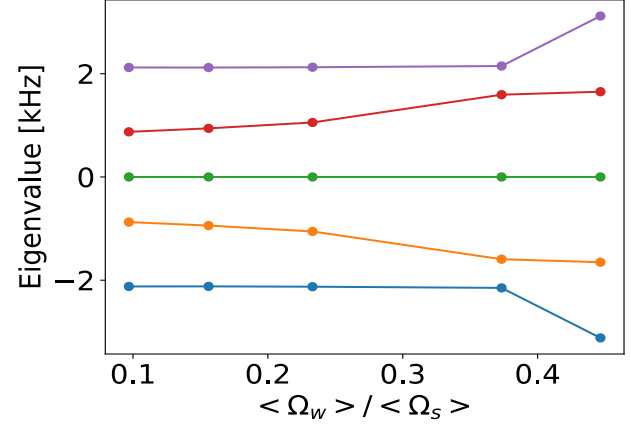
Extended Data Table I: **Rabi frequencies for the 3-site experiment in units of kHz.**



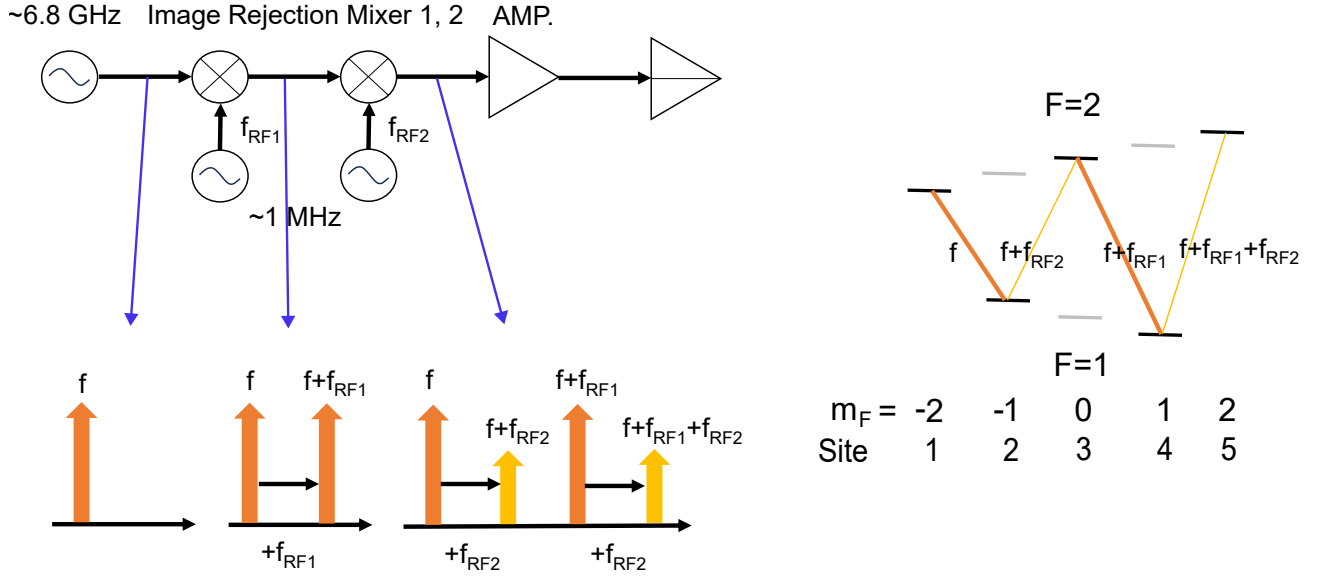
Extended Data Figure 1: **Experimental setup.** The configurations of the optical trap, the microwave irradiation and probe axis as well as coils for Stern-Gerlach separation are shown.

$\langle \Omega_W \rangle / \langle \Omega_S \rangle$	site	site 1 - 2 ( $\Omega_S^{(1)}/2\pi$ )	site 3 - 4 ( $\Omega_S^{(2)}/2\pi$ )	site 2 - 3 ( $\Omega_W^{(1)}/2\pi$ )	site 4 - 5 ( $\Omega_W^{(2)}/2\pi$ )
0.09691		2.119	0.8646	0.07464	0.1319
0.1560		2.116	0.8605	0.1081	0.3847
0.2331		2.120	0.8625	0.1379	0.6114
0.3733		2.123	1.363	0.2387	0.8563
0.4466		3.092	0.8446	0.3787	1.424

Extended Data Table II: **Rabi frequencies for the 5-site experiment in units of kHz.**

**a****b**

Extended Data Figure 2: **Numerical solutions to the 5-site SSH Hamiltonian.** **a**, Solutions to the 5-site SSH Hamiltonian (Eq. 3) with  $\Omega_i^{(1)} = \Omega_i^{(2)} = \Omega_i$  ( $i = S, W$ ) and  $\delta = 0$ . (top) Dependence of the Eigenenergies on the ratio  $\Omega_W/\Omega_S$  and (bottom) eigenvectors for several Rabi frequency ratio are plotted. **b** Solutions to the experimentally realistic Hamiltonian. Imbalance between  $\Omega_i^{(1)}$  and  $\Omega_i^{(2)}$  are considered and the dependence on their averaged values are shown. Characteristic features of the edge state, zero-energy and vanishing amplitude on the site 2 and 4, are retained.



Extended Data Figure 3: **Schematic of the microwave setup.** Two RFs are mixed to the main microwave by image rejection mixers (left). The frequency components at several stages are also shown. The resulting microwave has four frequency components set on-resonant to the transition involved in the 5-site experiment, as shown in the ground state energy diagram of  $^{87}\text{Rb}$  (right). In this configuration,  $\Omega_W$  can be controlled by the strength of RF2.